Numerical analyses of a PEM fuel cell's performance having a perforated type gas flow distributor

Muhammad. S. Virk[a], Mohamad Y. Mustafa[b] and Arne. E. Holdø[a]

[a]Department of Computer Science, Electrical Engineering and Space Technology, Narvik University College, Narvik 8505, Norway
[b]Energy & Environmental Technology Applied Research Group, Coventry University, Coventry CV1 5FB, UK
E-mail: msv@hin.no

ABSTRACT

This paper presents the steady state, isothermal, three dimensional (3D) numerical analyses of an intermediate temperature, proton electrolyte membrane (PEM) fuel cell's performance with the perforated type gas flow channels. Finite element based numerical technique is used to solve this multi transport numerical model coupled with the flow in porous medium, charge balance, electrochemical kinetics and membrane water content. Numerical analyses provided a detailed insight of the various physical phenomena, affecting this type of PEM fuel cell's performance. Results obtained from numerical analyses are compared with the experimental data and a good agreement is found. To validate this new design concept a comparison study is also carried out with the conventional PEM fuel cell having a serpentine type gas distributor. Results showed a better distribution of reactant species in the case of the perforated type gas distributor.

Key Words: PEM fuel cell, perforated, Serpentine, Isothermal, Single Phase, CFD,

1 INTRODUCTION

Among the different types of fuel cell, polymer electrolyte membrane (PEM) type fuel cells are considered most promising due to their efficiency, light weight and low operating temperature [1,2]. PEM fuel cells can be used for various applications such as 3C (*computer, communication and consumer electronics*) equipment, vehicle power systems and stationary power generation [1]. Key issues limiting the wide spread commercialization of PEM fuel cells are their performance, membrane life and high cost [3,4]. Performance of a PEM fuel cell can considerably be influenced by customizing the fluid flow behaviour along its domain. Major part of the previous research in the PEM fuel cell area is focused on the electro-chemistry and in particular on the performance of the proton electrolyte membrane. No major research activity has been carried out so far on improving the performance of the PEM fuel cell by optimizing the thermo-fluid properties [5].

One way of investigating fuel cell performance is by experiments, while other methods include numerical modelling [6-8]. Experimental procedures are expensive and have limitations in giving an insight of the transport phenomena; while numerical modelling can give a detailed picture of the flow behaviour, provided that the modelling process is mathematically and numerically correct. Various experimental and numerical studies have been

carried out by researchers during the past decades to investigate and improve the fundamental understanding of complex phenomena related to PEM fuel cell's performance [1,9]. Bernardi et al. [10] and Springer et al. [11] started to work on one dimensional isothermal numerical models of the PEM fuel cell. Later Newman and Fuller [12] developed a two dimensional model to study the water effects and thermal management related issues of the fuel cell, while Nguyen and White [13] employed a semi analytical solution procedure that included the effect of heat transfer in the fuel cell by prescribing the cell temperature and computing the heat transfer in the gas channels [14]. Baschuk and Kakac [15,16] studied variable degrees of water flooding in the catalyst layers and electrode backing regions. Wang et al. [17], Yu and Ferng et al. [1,18] proposed multi-component two phase transport models of the PEM fuel cell. Wang et al. also [19,20] worked on a 2D transient numerical model and studied the change of current density with changing cell potential. Wang also extended this work to third dimension and studied the effect of flow channel geometry and layout on the over all performance [6,19].

This paper primarily focuses on design, validation and performance analysis of a PEM fuel cell with novel design concept of a stainless steel made perforated type gas flow channel (meshed plate) instead of the conventional graphite made fuel cell gas flow channels such as parallel, spiral or serpentine shape. For the conventional gas flow channels, significant efforts and accuracy are required to machine and manufacture, depending on the complexity of the gas channel design topology, while the perforated type gas flow channel (Figure-01) are readily available in the market and can be customized according to the required design of the fuel cell. This design approach is more compact than the standard graphite-made gas flow channels due to the thickness and robustness of the stainless steel plates under machining and operating conditions. Moreover; in this design approach, membrane and stainless steel electrodes can be assembled as a single sealed unit that makes it simple and easy to replace in the case of any fault (Figure 1).

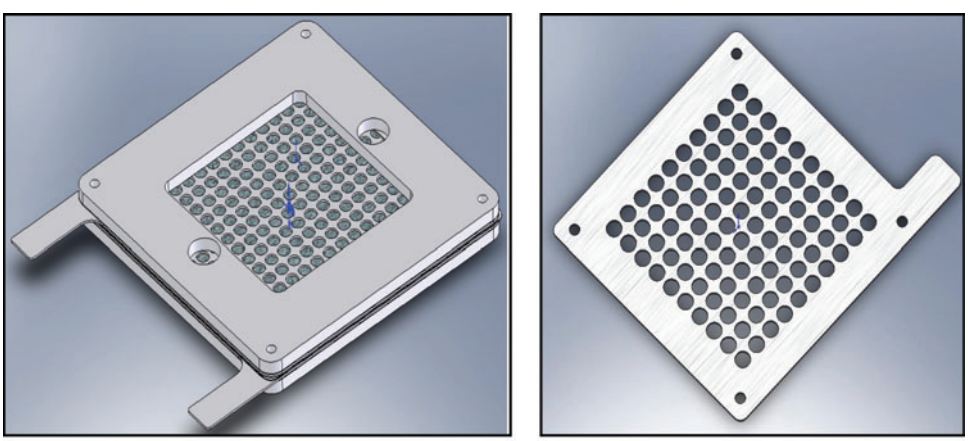

Figure 1 3D CAD model of PEM fuel cell with stainless steel made perforated type gas distributor.

The main objective of this research work is to simplify the design of the PEM fuel cell by optimizing the thermo-fluid properties of the reactant fluid flow along its domain, instead of dealing with the complex electro-chemical properties of the membrane electrode assembly of the PEM fuel cell. Around 50% increase in the performance has been reported just by the appropriate distribution of the reactant species along the fuel cell domain [21]. Detailed

numerical analyses are carried out to explore the insight of this new design concept, which are presented in the following sections.

2 MODEL DESCRIPTION

A PEM fuel cell, with an effective area of 25 cm^2, based on a stainless steel made perforated type gas flow distributor is used for this study, where hydrogen and oxygen served as fuel and reactant gases respectively. The flow direction of fuel at the anode side is taken opposite to that of the reactant gas at the cathode side. For numerical modelling, a three dimensional (3D) fully coupled numerical model is used, that resolved coupled transport phenomena of PEM fuel cell and accounted for the distributed over-potential at the catalyst layer as well as convention and diffusion of different species in the gas channels and in the porous gas diffusion layer (GDL). Whereas for experimental study the test facility (rig) used, was designed and assembled locally at the *'Energy and Environmental Technology Applied Research Group, Coventry University UK'*. Figure 02 shows a schematic over view of 3D-CAD model of this novel PEM fuel cell design, where the fuel cell domain is divided into seven layers: the gas channel, the perforated gas flow channel and the gas diffusion layer for both anode and cathode and a sandwiched membrane between both anode and cathode.

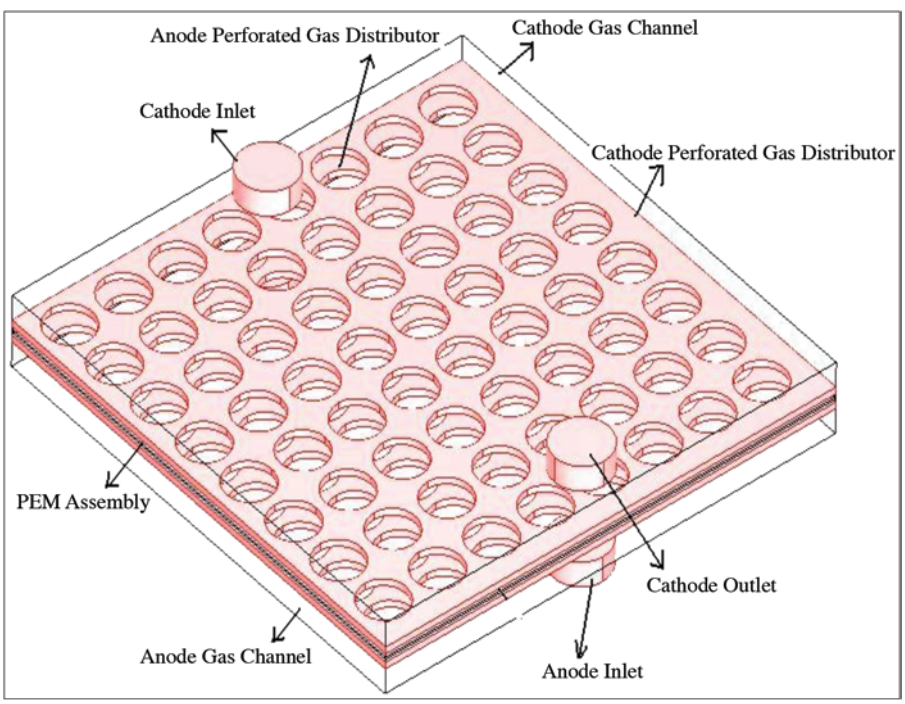

Figure 2 Schematic 3D-CAD Model of PEM fuel cell domain with perforated type gas flow channel, used for numerical analyses.

Physical and electrochemical phenomena that take place inside the PEM fuel cell are represented by the following governing equations, where the analyses are based on the solution of: conservation of mass, momentum, species and charge transport. Flow characteristics in the gas channels, perforated gas flow channel and porous media are obtained by solving the following form of the steady state Navier stoke equation: [3]

$$\nabla.\eta(\nabla u + (\nabla u)^T) + \rho(u.\nabla)u + \nabla p = 0 \tag{1}$$

Where as the reactant species transport in the PEM fuel cell domain is described by the divergence of mass flux through diffusion and convection, using the following form of mass transport equation [6]:

$$\nabla\left[-\rho w_i \sum_{j=1}^{N} D_{ij}\left\{\frac{\nabla M}{M_j}\left(\nabla w_j + w_j \frac{\nabla M}{M}\right) + \left(x_j - w_j\right)\frac{\nabla p}{p}\right\} + w_j \rho u\right] = 0 \tag{2}$$

Subscript 'i' denotes oxygen at the cathode and hydrogen at the anode sides, while 'j' is water vapour at both sides, 'w' is the mass fraction and 'ρ' is the gas mixture density that can be calculated by;

$$\rho = \frac{\sum x_i . MW_i}{RT} p \tag{3}$$

Diffusion coefficients of the reactant species 'D_{ij}' in non porous media are calculated by the Maxwell Stefan diffusion equation that accounts for coupling between the multi species components and the binary mass diffusion coefficients [3]

$$D_{ij} = \frac{T^{1.75}(1/M_i + 1/M_j)^{1/2}}{\rho((\sum_k V_{ki})^{1/3} + (\sum_k V_{kj})^{1/3})^2} \tag{4}$$

In order to account for the geometric constraints of the porous media, the diffusivities are corrected using the following Bruggemann correction formula [3,22]:

$$D_{ij}^{eff} = D_{ij} \times \varepsilon^{1.5} \tag{5}$$

Water management in the PEM fuel cell is critical and plays a vital role for its better performance. In addition to the molecular diffusion and electro-osmotic drag in the electrolyte membrane, water is generated due to the oxygen reduction reaction at the cathode catalyst layer [10]. Molar flux of water content 'α' in the PEM fuel cell membrane is based on the electro-osmotic drag coefficient 'n_d', water content 'λ' and water activity 'a' and is calculated using the following relations: [22,23]

$$\begin{aligned} a &= \frac{X_{H2O} P}{P_{sat}} \\ \lambda &= A_1 + A_2 a - A_3 a^2 + A_4 a^3 \qquad \text{for } 0 < a \le 1 \\ &\quad 14 + 1.4(a-1) \qquad \text{for } 1 \le a \le 3 \\ A_1 &= 0.043,\ A_2 = 17.18,\ A_3 = 39.85,\ A_4 = 36 \end{aligned} \tag{6}$$

Saturation pressure 'P', electro-osmotic drag coefficient 'n_d' and molar flux of water 'α' are calculated using the following relations [24]:

$$\log_{10} P_{sat} = -2.1794 + 0.02953(T - 273.15) - 9.1837 \times 10^{-5}(T - 273.15)^2$$
$$n_d = B_1\lambda + B_2\lambda - B_3$$
$$\alpha = \frac{n_d I_k}{F} - D_w \nabla C_w \tag{7}$$
$$B_1 = 0.0028,\ B_2 = 0.05,\ B_3 = 3.5 \times 10^{-19}$$

Membrane water diffusivity 'D_w' and water concentration 'C_w' across the membrane are calculated by [25,26]:

$$C_w = \frac{\rho_{mem,dry}}{M_{mem,dry}}\lambda \tag{8}$$
$$D_w = D_\lambda \exp\left[2416\left(\frac{1}{303} - \frac{1}{T}\right)\right]$$
where
$$D_\lambda = 10^{-10} \qquad \lambda < 2$$
$$D_\lambda = 10^{-10}(1 + 2(\lambda - 2)) \qquad 2 \le \lambda \le 3$$
$$D_\lambda = 10^{-10}(3 - 1.67(\lambda - 3)) \qquad 3 \le \lambda \le 4.5$$
$$D_\lambda = 1.25 \times 10^{-10} \qquad \lambda > 4.5$$

A potential difference exists between the catalyst and the electrolyte to drive the transfer current, keeping the electrochemical reaction continuous. The current passing through the catalyst layer can be decomposed into two parts, which interact through electrochemical reactions. Current fluxes at the cathode boundary between the electrode and the membrane are calculated using the following current conservation form [27]:

$$n.\left(-\sigma_{s,eff}\nabla\phi_s\right) = i_c$$
$$n.\left(-\sigma_{m,eff}\nabla\phi_s\right) = -i_c \tag{9}$$

$$n.\left(-\sigma_{s,eff}\nabla\phi_s\right) = -i_a$$
$$n.\left(-\sigma_{m,eff}\nabla\phi_s\right) = i_a \tag{10}$$

To express the relation between the local transfer current densities (j), the reactant concentrations (c_i) and the phase potentials, the following form of Butler-Volmer equation is used:

$$i_c = i_{oc}^{ref}\left(\frac{C_{o2}}{C_{o2}^{ref}}\right)\left[\exp\left(\frac{\alpha_c F}{RT}\eta_{act,c}\right) - \exp\left(-\frac{\alpha_c F}{RT}\eta_{act,c}\right)\right]$$
$$i_a = i_{oa}^{ref}\left(\frac{C_{H2}}{C_{H2}^{ref}}\right)^{\frac{1}{2}}\left[\exp\left(\frac{\alpha_a F}{RT}\eta_{act,a}\right) - \exp\left(-\frac{\alpha_a F}{RT}\eta_{act,a}\right)\right] \tag{11}$$

Where the activation over-potential 'η_{act}' at the cathode and anode is calculated by [27]:

$$\eta_{act,c} = \phi_s - \phi_m - V_{oc}$$

where

$$V_{oc} = 0.2329 + 0.0025T \qquad \text{(Reduces form of Nernst law)}$$

while

$$\eta_{act,a} = \phi_s - \phi_m$$

During these analyses; the catalyst layer is treated as a thin boundary interface, where sink and source terms for the reactants are implemented. Local volumetric sources and sink terms associated with the electrochemical reactions are proportional to the local current density and are calculated by [3,16]:

$$S_{H2} = -\frac{M_{H2}}{2F} i, \quad S_{O2} = -\frac{M_{O2}}{4F} i, \; S_{H2O} = \frac{M_{H2O}}{2F} i \tag{12}$$

2.1.1 Numerical setup

The governing equations together with their relative boundary conditions are solved using a commercial multi-physics numerical solver 'COMSOL v 3.4'. Convergence criterion is performed on each variable and the procedure is repeated until the convergence is obtained. All these numerical analyses are carried out considering the following assumptions:

a) Single Phase model as the water product is assumed to be in vapour form at operating conditions
b) Isotropic and Homogenous electrodes and membranes
c) Membrane impermeable for species in the gas phase
d) Negligible contact resistance
e) Negligible membrane swelling
f) Catalyst layer assumed as a reactive boundary layer.

Boundary conditions for the numerical model are specified at all external boundaries as well as boundaries for various mass transport and scalar equations inside the computational domain of the PEM fuel cell. The following points highlight the boundary conditions used for this numerical study.

- At both anode and cathode gas flow channel inlets, velocity, temperature and species mass fractions are specified as boundary conditions, whereas at outlet of the gas flow channel atmospheric pressure and convective flux boundary conditions are specified for species and thermal transport equations.
- No slip boundary condition is specified at the gas flow channel outer walls, which were also impervious to specious flow and thermally insulated (assumed).
- Continuous boundary is assumed between the gas flow channel and the perforated gas distributor open channels, while the solid section of the perforated gas distributor wall is used as boundary condition between the gas channel and perforated gas distributor.
- At the gas diffusion/catalyst layer interface, continuity is assumed as boundary condition.

- Mass flux of the reactant species is used as boundary condition at the membrane/catalyst layer interface for both anode and cathode sides due to electro-chemical reaction.
- The solid phase potential is arbitrarily set to zero as a reference at anode, while at cathode side, cell potential is set to $E_{cell} - E_{rev}$, where E_{cell} is the desired cell potential and E_{rev} = 1.14 V is the reversible cell potential. Moreover the cell potential gradient is set to zero at both catalyst layer/membrane interfaces, since there exists no solid phase current in the membrane.

3 RESULTS & DISCUSSION

This section presents the detailed performance analyses of a PEM fuel cell having stainless steel made perforated gas distributor, using a numerical approach. These numerical analyses are carried out assuming steady state isothermal flow conditions. Operating and geometric properties used for these analyses are specified in Tables 01 to 03. Both hydrogen and reactant air are assumed as counter flow. Numerical analyses of the velocity profile along the fuel cell domain shows that the reactant flow follows the shortest possible way from the inlet to the outlet of the fuel cell. Such flow behaviour leads to some dead zones at the corners of this type of PEM fuel cell. Figure-03 shows the velocity vectors near the inlet and the outlet sections of the fuel cell.

After passing from the inlet hole, The reactant flow gets spread along the rectangular gas channel. After they spread out along the gas channels, the reactant flows pass through the holes of the perforated plate, to get distribute along the porous gas diffusion layer (GDL) of the PEM fuel cell. For perforated type gas flow channel, this distribution is strongly influenced by effective open area of the perforated plate. During this study a perforated plate with an effective open area of 55% is used, where the diameter of each perforated hole is 2.5 mm. 45% area of the perforated plate is covered that means a low mass fraction of reactant species can be found under the covered area of the perforated gas flow channel. Detailed analyses are carried out to analyse the distribution of reactant species along this new design of PEM fuel cell. Figure 04 shows the distribution of oxygen and water mass fraction along cathodes side of the PEM fuel cell at V = 0.5 Volts.

Table 1 Geometrical parameters of PEM fuel cell for numerical simulations

Parameter	Value	Unit
Gas Channel length	0.05	m
Gas Channel width	0.002	m
Perforated sheet Thickness	0.00055	m
Perforated Hole Diameter	0.003	m
GDL Thickness	0.0002	m
Membrane Thickness	0.00018	m

Table 2 Material properties for stainless steel 316L

Parameter	Value	Unit
Electrical Resistivity	7.493e-7	Ω-m
Thermal Conductivity	15	W/m-K
Heat Capacity	502	J/Kg-K
Co-efficient of thermal expansion	1.6e-5	1/K
Density	7889	Kg/m^3

Table 3 Operating parameter conditions for numerical analyses

Parameters	Value	Unit
Oxygen Inlet Mass Fraction	0.226	
Water Inlet Mass Fraction	0.0934	
Hydrogen Inlet Mass Fraction	0.844	
Operating Temperature	333	K
Inlet Pressure	101325	Pa
Relative Humidity, Air	70%	
Relative Humidity, H2	92%	
Electrode electronic conductivity	120	S/m
Membrane ionic conductivity	17.69	S/m
Transfer Coefficient, cathode side	0.5	
Transfer Coefficient, anode side	0.5	
Cathode reference exchange current density	1.0E-02	A/cm^2
Anode reference exchange current density	1.00E+04	A/cm^2
Concentration Parameter, Cathode	1	
Concentration Parameter, Anode	0.5	
Gas diffusion layer porosity	50%	
GDL Hydraulic Permeability	1.79e–11	m^2

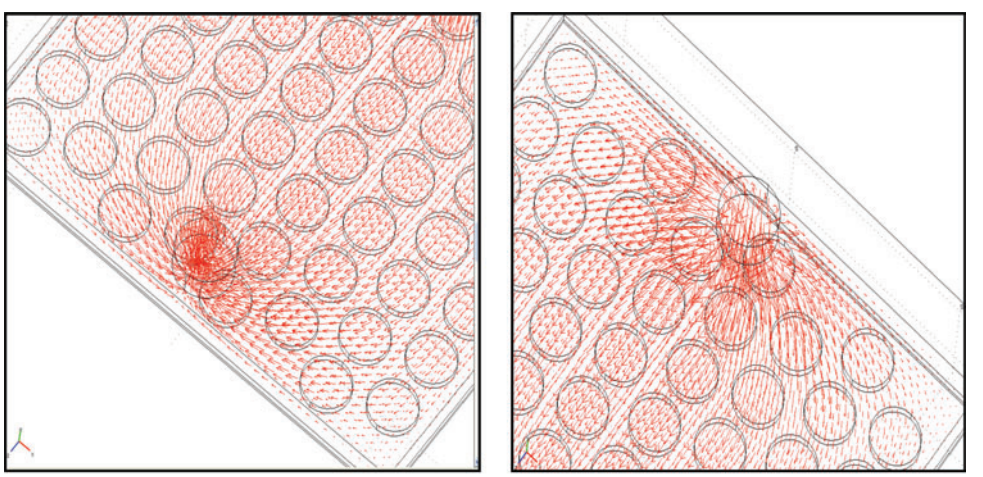

(Near outlet) (Near inlet)

Figure 3 Velocity vectors, near inlet/outlet sections of the PEM fuel cell highlighting the velocity profile and dead zones at corners of the computational domain.

Figure 04 shows a high mass fraction of oxygen near the inlet section, while a low mass fraction of oxygen is observed near out let section due to its consumption during electro-chemical reaction along cathode catalyst layer. After passing through the gas diffusion layer, the reactant species reach at catalyst layer, where hydrogen and oxygen get split into their constituents and an electrochemical reaction takes place between reduced oxygen and protons at cathode catalyst layer.

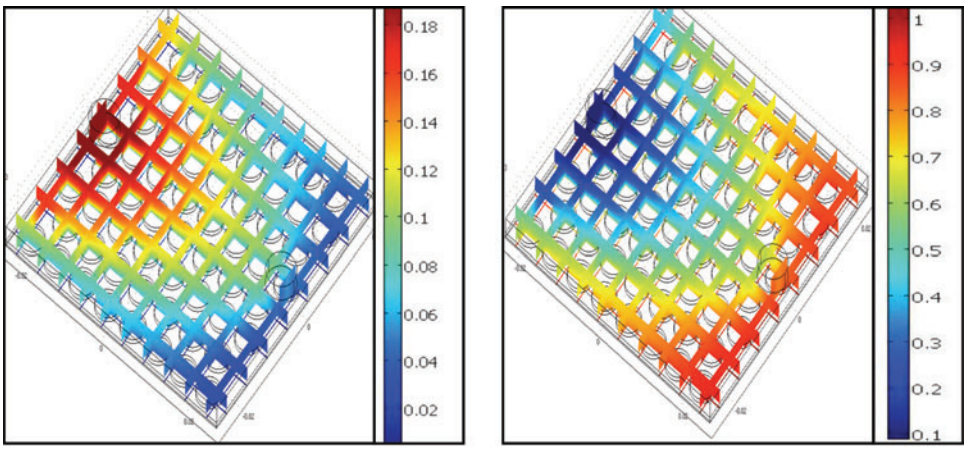

(Oxygen mass fraction) (Water mass fraction)

Figure 4 Distribution of oxygen and water mass fraction along cathode side of the

Anode Reaction: $2H_2 \rightarrow 4H^+ + 4e^-$ (eq-1)

Cathode Reaction: $O_2 + 4H^+ + 4e^- \rightarrow 2H_2O$ (eq-2)

Overall Reaction: $O_2 + 2H_2 \rightarrow 2H_2O$ (eq-3)

Performance of the PEM fuel cell is strongly influenced by the distribution of reactant species along the cathode catalyst layer. High mass fraction of oxygen at cathode catalyst layer improves the electrochemical reaction that consequently enhance the over all performance. Water gets generate as by product of this electro-chemical reaction. Evaporation of this water is essential as water flooding can lead to a decreases in fuel cell performance. Numerical analyses of reactant species distribution along the cathode catalyst layer show a high mass fraction of oxygen below the open sections of the perforated plate, while a very low mass fraction of oxygen is observed below the solid sections of the perforated plate. Such distribution leads to a high water flooding below the solid sections of the perforated plate, due to the limited access of reactant air in these sections. Reactant air evaporates the excess water from the fuel cell domain. Figure 05 shows the distribution of oxygen and water mass fractions along cathode catalyst layer of the PEM fuel cell with perforated type gas distributor at V = 0.5 volts.

Figure-05 shows a high mass fraction of oxygen below the open sections near the inlet, while a low mass fraction is observed below the solid sections of the perforated plate and at corners of the fuel cell domain. This leads to high mass fraction of water in these area. Such distribution of reactant species highlights that effective open area of the perforated plate plays a vital role towards better distribution of reactant species along the catalyst layer and consequently on the overall performance of the PEM fuel cell. Numerical analyses of current density distribution along the cathode catalyst layer due to the electro-chemical reaction shows a high value of current density below the open areas of the perforated plate, where the

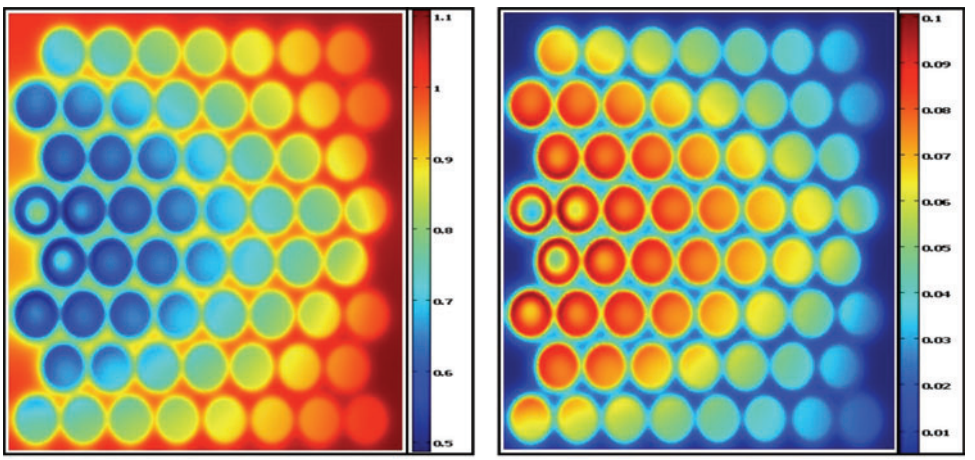

Figure 5 Distribution of oxygen and water mass fractions along cathode catalyst layer of the PEM fuel cell at V = 0.5 Volts, T = 60 C°.

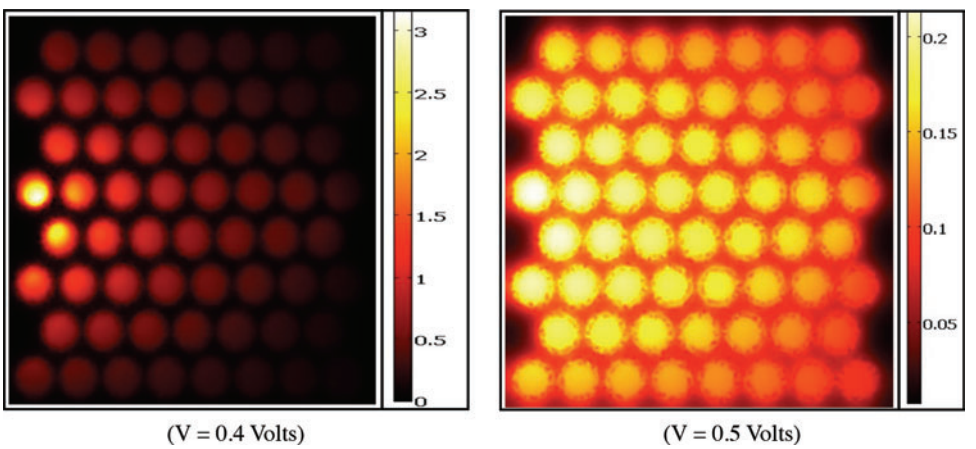

Figure 6 Current density distribution along the cathode catalyst layer at different load conditions.

high mass fraction of oxygen was observed. Figure 06 shows the distribution of current density along the cathode catalyst layer at V = 0.4 and 0.5 volts.

To validate the numerical model, numerical results are compared with the experimental data at different load conditions. At this point, it should be noted that at present the polarization curve is the only experimental data that is available in the literature to compare with the numerical data. Therefore the polarization curves are commonly used by researchers to confirm the agreement between numerical and experimental models. Strict validation would require detailed data comparison from local distribution of the current densities, species concentration and distribution etc along the

fuel cell domain, but such data is very difficult to obtain from the experiments, therefore the polarization curve is used here to make a comparison between the numerical and the experimental results. Figure 07 shows the performance polarization curves of this new design of PEM fuel cell at T = 60 ˚C. Results showed a good agreement at both low and intermediate current densities, but at higher current densities due to one-phase nature of the numerical model, the effect of reduced oxygen transport due to water flooding at the cathode is not accurately accounted.

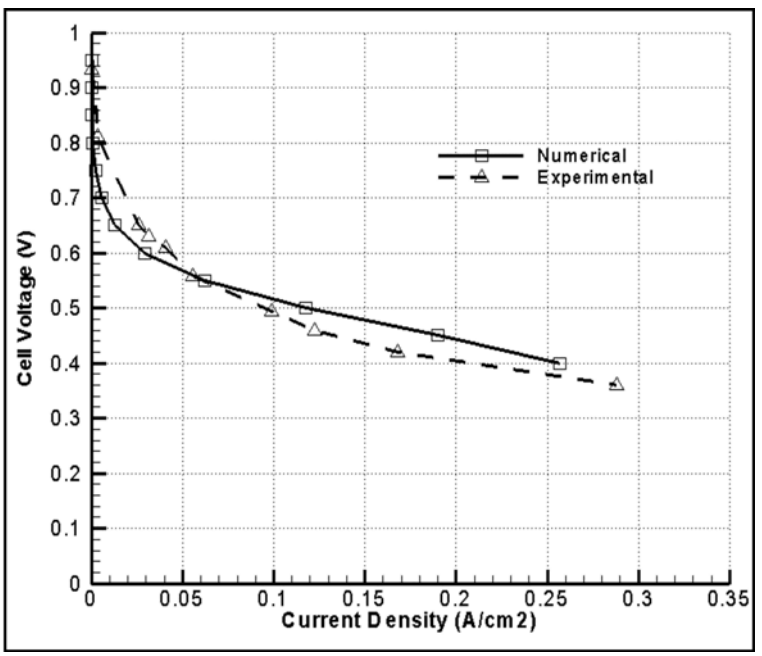

Figure 7 Comparison of polarization curves for the experimental and numerical models of the PEM fuel cell with perforated type gas distributor, at T = 333K

To validate the design concept of the perforated type gas distributor a comparison study is also carried out with a graphite based PEM fuel cell having serpentine shaped gas flow channels. For the perforated type gas flow channels; the reactant flow enters form the inlet and then freely spread out along the gas channel and consequently passes through the perforated holes. In the case of serpentine shaped gas channels, flow is not free to move around. It moves in narrow gas channels, where the side wall effects are considerable. These side wall effects do not allow the reactant flow to move smoothly form the inlet to the outlet section. The major part of the reactant species gets consumed near the inlet section. This leads to an uneven distribution of the reactant species. To overcome this issue; a high pressure flow is required in the case of serpentine shaped gas flow channels to move completely from the inlet to the outlet port. An alternative way is to increase the size of the gas channels, but this will be at additional

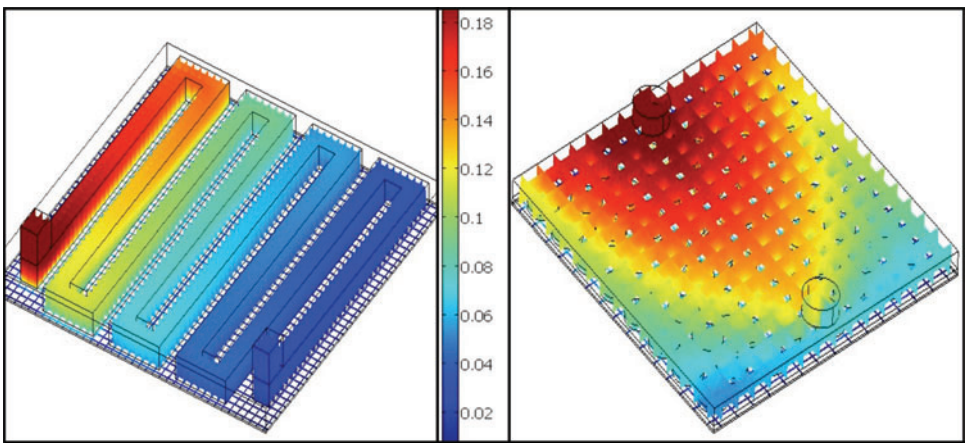

Figure 8 Oxygen mass fraction distribution along the cathode side of the PEM fuel cell in the case of serpentine and perforated type gas flow channels at V = 0.5 Volts, T = 333 K

cost to the system. Such behaviour of the reactant flow effects the distribution of the reactant species along the fuel cell domain**.** Results show a better distribution of reactant species along the fuel cell domain in the case of perforated type gas distributor. Figure 08 shows the oxygen mass fraction distribution along cathode side of the PEM fuel cell in both design configurations. Such distribution of reactant species effectively improves the performance of the fuel cell. Figure 09 shows the performance polarization curves for both design configurations.

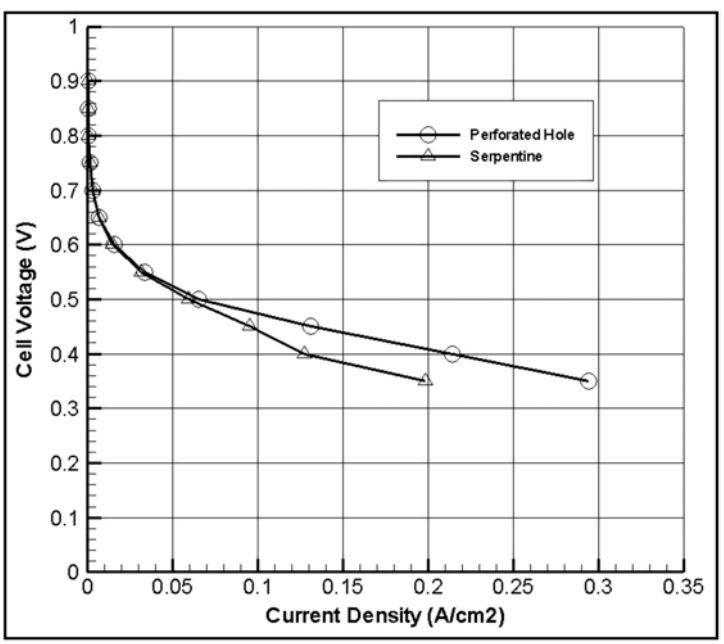

Figure 9 Comparison of PEM fuel cell performance with perforated and serpentine type gas flow channels at T = 333 K

ACKNOWLEDGEMENT

The authors would like to acknowledge the kind guidance of Prof F. S. Bhinder and Mr Ali Abul Hawa. Their Valuable professional advice and comments were motivating and inspiring throughout this research work.

NOMENCLATURE

ρ = Density (kg/m^3)
u = Velocity (m/s)
η = Viscosity (kg/m-s)
p = Pressure (Pa)
D = Diffusion Coefficient (m^2/s)
T = Temperature (K)
v = Molar Diffusion Volume of species (m^3/mol)
M = Molar Masa
k_p = Permeability (m^2)
ε = Porosity
σ = Ionic Conductivity (S/m)
φ = Cell Potential (V)
i = Current Density (A/ cm^2)
i_o = Reference Exchange Current Density
F = Faraday Constant, = 96747 (C/mol)
R = Universal Gas Constant, = 8.314 (J/mol-K)
$C_{o2,ref}$ = Local Oxygen Concentration (mol/m^3)
$C_{H2,ref}$ = Local Hydrogen Concentration (mol/m^3)
n = Number of electron transfer
w = Weight Fraction
a = Water Activity
λ = Membrane Water Contents

REFERENCE

1. Ferngа, Y.M., A. Su, and S.M. Lu, *Experiment and Simulation investigations for effect of flow channel patterens on PEMFC Paerfromance.* International Journel of Energy Research, 2008. **32**: p. 12–23.
2. YING and M. Ouyang, *Three Dimensional Heat and Mass Transfer analysis in an air-breathing Proton Exchange Membrane Fuel Cell.* jounal of Power source, 2007. **164**: p. 721–729.
3. MARS, A. and A. HAKS, *Parametric and optimization study of a PEM fuel cell performance using three-dimensional computational fluid dynamics model.* Renew Energy, 2007. **32**: p. 1077–1101.
4. Hontanon, M.J. Escudero, and C. Bautista, *Optimisation of flow-field in polymer electrolyte membrane fuel cells using computational fluid dynamics techniques.* Journal of Power Sources, 2000. **86**: p. 363–68.
5. Chu, H.S., F. Tsau, and Y.Y. Yan, *The development of a small PEMFC combined heat and power system.* journal of power sources, 2008. **176**(2): p. 499–514.
6. Wang, C.-Y., *Fundamental Models of Fuel cell Engineering.* Chem Rev, 2004. **104**: p. 4727–4766.
7. Ren, G.P. and L.J.Y. Qin, *Transport Mechanisims and Performance Simulation of PEM Fuel Cell.* International Journal of Energy Research, 2008. **32**: p. 514–530.

8. Djilalib, N. and B.R. Sivertsena, *Computational modelling of polymer electrolyte membrane (PEM) fuel cells: Challenges and opportunities.* Energy, 2007. **32**: p. 269–280.
9. Carcadea, E., H. Ene, and Ingham, *A Computational Fluid Dynamics Analysis of a PEM Fuel Cell System for Power generation.* International Journal of Numerical Methods for Heat and Fluid Flow, 2007. **17**(3): p. 302–312.
10. Bernardi, D.M. and M.W. Vebrunge, *A mathematical model of the solidpolymer electrolyte fuel cell.* Journal of Electrochemical Society, 1992. **139**(9): p. 2477–2491.
11. Springer, T.E., T.A. Zawodzinski, and S. Gottesfeld, *Polymer electrolyte fuel cell model.* J. Electrochem. Soc., 1991. **138**(8): p. 2334–2342.
12. Fuller, T.F. and J. Newman, *Water and thermal management in solid-polymer electrolyte fuel cells,.* Journal of Electrochemical Society, 1993. **150**(5): p. 1218–1225.
13. Nguyen, T.V. and R.E. White, *A Water and Heat Management Model for Proton-Exchange-Membrane Fuel Cells,".* Journal of the Electrochemical Society, 1993. **140**: p. 2178–2186.
14. Shawn Edward Litster, *Mathematical Modelling of Fuel Cells for Portable Devices*, in *Department of Mechanical Engineering*. 2004, University of Victoria,. p. 156.
15. Baschuk, J.J. and X. Li, *Modeling of polymer electrolyte membrane fuel cells with variable degrees of water flooding.* Journal of Power Sources, 2000. **86**: p. 181–196.
16. Gurau, V., H. Liu, and S. Kakac, *Two-dimensional model for proton exchange membrane fuel cells.* AIChE J, 1998. **44**(11): p. 2410–2422.
17. Wang, Z., W. CY, and C. KS, *Two phase flow and transport in the air cathode of proton exchange membrane fuel cells.* jounal of Power source, 2002. **94**: p. 40–50.
18. Ferng, Y., *Analytical and experimental investigations of a Proton Exchange Membrane fuel cell.* International Journal of Hydrogen Energy, 2004. **29**: p. 381–391.
19. Wang and K.S. Chen, *Computational fluid dynamics modeling of proton exchange membrane fuel cells,.* J. Electrochem. Soc., 2000. **147**(12): p. 4485–4493.
20. Shimpalee and S. Dutta, *Effect of Humidity on PEM Fuel Cell Performance. Part II. Numerical Simulation,.* Heat Transfer Divison , ASME, 1999. **364–1**.
21. Watkins, D.S., *Novel fuel cell Fluid flow field plate.* US Patent 4988583, 1991.
22. Chen, F., M.H. Chang, and C.F. Fang, *Analysis of Water Transport in a Five Layer Model of PEMFC.* jounal of Power source, 2007. **164**: p. 649–658.
23. Nguyen, B. T, and D. N, *Computational model of a PEM fuel cell with serpentine gas flow channels.* J Power Sources, 2004. **130**: p. 149–57.
24. Meng, H., *A Three Dimensional Mixed Domain PEM Fuel Cell model with fully Coupled Transport Phenomena.* jounal of Power source, 2007. **164**: p. 688–696.
25. Djillali, N. and T. Bearing, *Three dimensional computational analyses of transport phenomena in PEM fuel cell-a parametric study.* jounal of Power source, 2003. **124**: p. 440–452.
26. Motupally, S., A.J. Becker, and J.W. Weidner, *Diffusion of water in Nafion 115 membranes,.* J. Electrochem. Soc., 2000. **147**(9): p. 3171.
27. Guvelioglu, G.H. and H.G. Stenger, *Computational fluid dynamics modeling of polymer electrolyte membrane fuel cells.* Journal of Power Sources, 2005. **147**: p. 95–106.